Motion of Charged Particles around a Weakly Magnetized Rotating Black Hole

Ryo Shiose,[1] Masashi Kimura,[2] and Takeshi Chiba[1]

[1]*Department of Physics, College of Humanities and Sciences, Nihon University, Tokyo 156-8550, Japan*
[2]*DAMTP, University of Cambridge, Centre for Mathematical Sciences, Wilberforce Road, Cambridge CB3 0WA, UK*

(Dated: November 18, 2014)

We study the motion of a charged particle around a weakly magnetized rotating black hole. We classify the fate of a charged particle kicked out from the innermost stable circular orbit. We find that the final fate of the charged particle depends mostly on the energy of the particle and the radius of the orbit. The energy and the radius in turn depend on the initial velocity, the black hole spin, and the magnitude of the magnetic field. We also find possible evidence for the existence of bound motion in the vicinity of the equatorial plane.

PACS numbers: 04.70.Bw, 04.25.-g, 04.70.-s , 97.60.Lf

arXiv:1409.3310v3 [gr-qc] 17 Nov 2014

I. INTRODUCTION

Black holes (BHs) are ubiquitous in the Universe and play an important role in the formation of galaxies [1]. BHs produce intense radiation by converting the gravitational binding energy of accreting plasmas [2]. Accreting BHs immersed in large-scale magnetic fields also release their rotational energy into powerful relativistic jets [3], which are observed in active galactic nuclei, quasars, or X-ray binaries. Numerical simulations demonstrated that powerful jets are generated by extracting energy from a spinning BH along the magnetic field [4].

Moreover, the power of jets from BHs with thick accretion disks depends mostly on BH spin, which may explain the wide variety of radio luminosities of active galactic nuclei [5]. BH spin is measured by the X-ray reflection method [6] (see [7] for a recent review) and by the continuum-fitting method [8] (see [9] for a recent review), and it is found that a large fraction of astrophysical BHs are rapidly rotating.

In this paper, in order to examine the effects of a magnetic field and BH spin on particle motion, we investigate the motion of a charged particle around a rotating black hole in a uniform magnetic field. Although this is a simplified problem, the dynamics are still nonintegrable due to the lack of a third constant of motion (the Carter constant) in the presence of a magnetic field. If we focus on equatorial motion, a semi-analytical approach is possible [10–12], but a general orbit requires numerics [13–17]. More specifically, we consider the motion of a charged particle kicked out from the equatorial plane, and investigate the conditions under which such a particle can escape to infinity. This problem was studied in [13, 14, 16, 18] for a nonrotating black hole and in [15] for a slowly rotating black hole. There, it was found that the charged particle is either captured by the black hole, or escapes in a direction parallel or antiparallel to the magnetic field. The final fate of this particle is extremely sensitive to the initial conditions determined by the strength of the magnetic field. Since astrophysical BHs are rotating (sometimes rapidly), we extend such an analysis to a rotating black hole.

The paper is organized as follows. In Sec. II, after introducing a uniform magnetic field, we present the equations of motion for a charged particle and study the innermost stable circular orbits. In Sec. III, we present the results of numerical calculations for particles kicked out of these innermost stable circular orbits and discuss the final fate of the particles. We summarize our results in Sec. IV.

Appendix A contains an analysis of the magnetic flux across a black hole for two field configurations. In Appendix B, we present approximate solutions for the innermost stable circular orbits. We use units in which $G = c = 1$.

Note added: during the preparation of our paper, we became aware of a work on similar topics [19]. While it has some overlaps with our paper, the analysis of motion of a particle kicked out from a circular orbit in [19] is limited to a fixed value of a magnetic field. Our analysis is complementary to the results of [19].

II. WEAKLY MAGNETIZED ROTATING BLACK HOLE

We consider the motion of charged particles in a weakly magnetized rotating black hole. By "weakly magnetized," we mean that the energy density of the magnetic field does not significantly distort the background black hole geometry which is assumed to be given by the Kerr metric (in the Boyer-Lindquist coordinates),

$$\begin{aligned} ds^2 &= g_{\mu\nu}dx^\mu dx^\nu \\ &= -\left(1-\frac{2M}{\Sigma}\right)dt^2 - \frac{4aMr\sin^2\theta}{\Sigma}dtd\phi + \frac{\Sigma}{\Delta}dr^2 + \Sigma d\theta^2 + \frac{(r^2+a^2)^2 - a^2\Delta\sin^2\theta}{\Sigma}\sin^2\theta d\phi^2 \end{aligned} \tag{1}$$

where M is the gravitational mass of the black hole and a is its angular momentum per unit mass and $\Sigma = r^2 + a^2\cos^2\theta$ and $\Delta = r^2 + a^2 - 2Mr$. The event horizon is located at $r_H = M + \sqrt{M^2 - a^2}$.

The effect of the magnetic field on the background geometry can be neglected if

$$GB^2 \ll (GM)^{-2} \quad \text{or} \quad B \ll G^{-3/2}M^{-1} \sim 10^{19}\text{Gauss}(M_\odot/M), \tag{2}$$

where we have momentarily restored the gravitational constant G for clarity. This condition is satisfied for astrophysical black holes (typically $< 10^9$Gauss [20]). Therefore, the magnetic field can be considered as a test field in the background geometry. Although the magnetic field is "weak" compared with the background, it can be quite "strong" for charged particles. This can be seen by taking the ratio of the Lorentz force to the gravitational force acting on a charged particle with charge q and the rest mass m in the Keplerian orbit. For the radius close to the Schwarzschild radius, the ratio becomes

$$\frac{qBM}{m} \sim 10^6 \left(\frac{q}{e}\right)\left(\frac{B}{10^8\text{Gauss}}\right)\left(\frac{M}{M_\odot}\right)\left(\frac{m_p}{m}\right), \tag{3}$$

where m_p is the mass of proton. Thus it can be quite large for charged particles (protons or electrons) around astrophysical BHs.

A. Black Hole in a Uniform Magnetic Field

As long as the magnetic field can be treated as a test field, we can choose any field configuration we like. However, for a Ricci flat spacetime with Killing vectors, it is well known that a Killing vector solves the Maxwell equation for a 4-vector potential A^μ in the Lorenz gauge: $\nabla_\mu A^\mu = 0$. The Kerr spacetime is stationary and axisymmetric with Killing vectors $\xi^\mu = (\partial/\partial t)^\mu$ and $\psi^\mu = (\partial/\partial\phi)^\mu$. Therefore, A^μ is a linear combination of these Killing vectors. In particular, as shown by Wald [21], for a neutral rotating black hole, the special choice

$$A^\mu = \frac{B}{2}\left(\psi^\mu + 2a\xi^\mu\right) \tag{4}$$

generates an asymptotically uniform magnetic field of strength B. However, the second term in Eq. (4) is the effect of Faraday induction due to the rotation of a BH, which generates a difference in the electrostatic potential between the event horizon and infinity. Consequently, positively charged particles are accreted towards the horizon. For a charged rotating black hole with charge Q, Eq. (4) becomes

$$A^\mu = \frac{B}{2}\left(\psi^\mu + 2a\xi^\mu\right) - \frac{Q}{2M}\xi^\mu\,. \tag{5}$$

Thus, the accretion continues until the potential difference disappears and the black hole will acquire an inductive charge of $Q = 2aMB$ [10, 21]. After the accretion is complete, the 4-vector potential becomes

$$A^\mu = \frac{B}{2}\psi^\mu\,. \tag{6}$$

Note that as long as the condition Eq. (2) is satisfied, the induced charge of the black hole is so small $Q/M = 2aB \leq 2BM \ll 1$ that its effect on the background black hole geometry can be neglected. Hence, we shall adopt this choice of 4-vector potential Eq. (6) together with the background black hole geometry Eq. (1).[1] In Appendix A, we calculate the magnetic flux across a black hole for two typical field configurations Eqs. (4) and (6).

B. Motion of Charged Particles

The equation of motion for a test particle of mass m and charge q is given by

$$mu^\nu\nabla_\nu u^\mu = qF^\mu{}_\nu u^\nu. \tag{7}$$

[1] The motion of charged particles for the choice of the magnetic field Eq. (4) was studied in [17].

Here, $u^\mu = \dot{x}^\mu \equiv dx^\mu/d\tau$ is the particle 4-velocity with τ being proper time and $u^\mu u_\mu = -1$. Also, $F_{\mu\nu} = \nabla_\mu A_\nu - \nabla_\nu A_\mu$ is the field strength. The equation is derived from the Lagrangian

$$L = \frac{1}{2} m g_{\mu\nu} u^\mu u^\nu + q A_\mu u^\mu \,, \tag{8}$$

from which the momentum p_μ conjugate to x^μ is defined by

$$p_\mu = m u_\mu + q A_\mu \,. \tag{9}$$

For a Kerr black hole immersed in the uniform magnetic field $B(>0)$, Killing fields ξ^μ and ψ^μ yield a conserved energy per rest mass $\mathcal{E}$ and an angular momentum per rest mass $\mathcal{L}$ for the motion of a charged particle

$$\mathcal{E} = -\frac{1}{m} p_\mu \xi^\mu = \left(1 - \frac{2Mr}{\Sigma}\right)\dot{t} + \frac{2aMr\sin^2\theta}{\Sigma}\left(\dot{\phi} + \frac{b}{2M}\right), \tag{10}$$

$$\mathcal{L} = \frac{1}{m} p_\mu \psi^\mu = -\frac{2aMr\sin^2\theta}{\Sigma}\dot{t} + \frac{(r^2+a^2)^2 - a^2\Delta\sin^2\theta}{\Sigma}\sin^2\theta\left(\dot{\phi} + \frac{b}{2M}\right), \tag{11}$$

where we have used Eq. (6) and introduced $b = qBM/m$ which is the ratio in Eq. (3) [2]. Hence, the azimuthal motion is integrable. We note that $\mathcal{E}$ and $\mathcal{L}/M$ are dimensionless quantities. In the presence of a magnetic field, we should carefully consider the meaning of $\mathcal{E}$ and $\mathcal{L}$ because they contain the magnetic field b in their definition. Solving Eqs. (10) and (11) in terms of $\dot{t}$ and $\dot{\phi}$, we obtain

$$\dot{t} = \frac{\left((r^2+a^2)^2 - a^2\Delta\sin^2\theta\right)\mathcal{E} - 2aMr\mathcal{L}}{\Delta\Sigma}, \tag{12}$$

$$\dot{\phi} = -\frac{b}{2M} + \frac{2aMr\mathcal{E} + (-a^2 + \Delta\csc^2\theta)\mathcal{L}}{\Delta\Sigma}. \tag{13}$$

When we discuss the motion of particles on and outside the black hole horizon, we must impose the forward-in-time condition $\dot{t} \geq 0$ which means that the value of the time coordinate t increases along the trajectory of the particle. The radial motion and the polar motion are obtained by solving the equation of motion Eq. (7),

$$\begin{aligned}\Sigma\ddot{r} &= -\frac{a^2 r\sin^2\theta + M(\Sigma - 2r^2)}{\Delta}\dot{r}^2 + a^2\sin(2\theta)\dot{r}\dot{\theta} + \Delta r\dot{\theta}^2 - \frac{b^2\Delta\sin^2\theta}{4M^2\Sigma^2}(r\Sigma^2 + a^2 M\sin^2\theta(\Sigma - 2r^2)) \\ &\quad + \frac{M(\Sigma - 2r^2)}{\Delta\Sigma^2}((a^2+r^2)\mathcal{E} - a\mathcal{L})^2 + \frac{r\sin^2\theta}{\Delta\Sigma^2}(a(2Mr\mathcal{E} - a\mathcal{L}) + \mathcal{L}\Delta\csc^2\theta)^2, \end{aligned} \tag{14}$$

$$\begin{aligned}\Sigma\csc(2\theta)\ddot{\theta} &= -\frac{a^2}{2\Delta}\dot{r}^2 - 2r\csc(2\theta)\dot{r}\dot{\theta} + \frac{a^2}{2}\dot{\theta}^2 - \frac{b^2}{8M^2\Sigma^2}\left(\Delta\Sigma^2 + 2Mr(a^2+r^2)^2\right) \\ &\quad + \frac{Mr(a\mathcal{E} - \mathcal{L}\csc^2\theta)^2}{\Sigma^2} + \frac{1}{2\Delta\Sigma^2}(a(2Mr\mathcal{E} - a\mathcal{L}) + \mathcal{L}\Delta\csc^2\theta)^2. \end{aligned} \tag{15}$$

We solve the above equations from a point $x^\mu = x^\mu_{\rm ini}$ with an initial velocity $\dot{x}^\mu = u^\mu_{\rm ini}$. Here we must choose $u^\mu_{\rm ini}$ so that it satisfies the normalization condition $g_{\mu\nu}u^\mu_{\rm ini}u^\nu_{\rm ini} = -1$ and the forward-in-time condition $u^0_{\rm ini} > 0$ if $r_{\rm ini} > r_H$. Since Eqs. (12) - (15) are invariant under the transformation $a \to -a, b \to -b, \mathcal{L} \to -\mathcal{L}$ and the redefinition of the polar coordinates $\bar{\theta} := \pi - \theta, \bar{\phi} := -\phi$, we only need to consider $a \geq 0$. While we need numerics to study the general orbits of charged particle, we can solve them analytically if we focus on an orbit in the equatorial plane $\theta = \pi/2$, as we will discuss in the next section.

C. ISCO

Let us consider particle motion in the equatorial plane. Then, the equation of motion becomes integrable, and from $u^\mu u_\mu = -1$ we obtain the equation for radial motion [10, 11]

$$r^3\dot{r}^2 = V(r, \mathcal{E}, \mathcal{L}, b), \tag{16}$$

---

[2] Note that our b differs from that in [13, 14] by a factor of 2, $b_{\rm ZFS} = b/2$.

where

$$V(r,\mathcal{E},\mathcal{L},b) \;=\; (r^3+a^2r+2Ma^2)\left(\mathcal{E}^2-\frac{b^2}{4M^2}\Delta\right)-(r-2M)\mathcal{L}^2-4Ma\mathcal{E}\mathcal{L}-r\left(1-\frac{b\mathcal{L}}{M}\right)\Delta\,. \tag{17}$$

The maximum of V determines the stable circular orbit and hence $V=\partial V/\partial r=0$ there. The innermost of such orbits is called ISCO (the innermost stable circular orbit), where relativistic effects heavily influences the motion of charged particles. The ISCO radius is determined by solving the equations $V=\partial V/\partial r=\partial^2 V/\partial r^2=0$. These were first solved by [10] and the results are

$$\mathcal{L}=-b\left(r-\frac{a^2}{3r}\right)\pm\sqrt{\lambda}\,, \tag{18}$$

$$\mathcal{E}^2=\eta\mp\frac{b}{M}\left(1-\frac{2M}{3r}\right)\sqrt{\lambda}\,, \tag{19}$$

which are derived from $\partial V/\partial r=\partial^2 V/\partial r^2=0$, where the upper sign ($\mathcal{L}>0$) refers to "prograde" (or anti-Larmor according to [10]) motion and the lower sign ($\mathcal{L}<0$) refers to "retrograde" (or Larmor) motion. We note that the sign of $\mathcal{L}$ does not necessarily coincide with the sign of $\dot{\phi}$. λ and η are defined by

$$\lambda=2M\left(r-\frac{a^2}{3r}\right)+\frac{b^2}{4M^2}\left(r^2\left(5r^2-4Mr+4M^2\right)+\frac{2}{3}a^2(5r^2-6Mr+2M^2)+a^4\left(1+\frac{4M^2}{9r^2}\right)\right), \tag{20}$$

$$\eta=1-\frac{2M}{3r}-\frac{b^2}{6}\left(4-5\frac{r^2}{M^2}-\frac{a^2}{M^2}\left(3-\frac{2M}{r}+\frac{4M^2}{3r^2}\right)\right)\,. \tag{21}$$

Putting Eqs. (18) and (19) into $V=0$ gives the equation for the ISCO radius r_I

$$(r^3+a^2r+2Ma^2)\left(\mathcal{E}^2(r)-\frac{b^2}{4M^2}\Delta\right)-(r-2M)\mathcal{L}^2(r)-4Ma\mathcal{E}(r)\mathcal{L}(r)-r\left(1-\frac{b\mathcal{L}(r)}{M}\right)\Delta\;=\;0. \tag{22}$$

In general, Eq. (22) can only be solved numerically. We identify the root of Eq. (22) which is the closest to r_H as the ISCO radius r_I, although there can be multiple solutions [10]. We can find the corresponding energy and angular momentum from Eqs. (18) and (19). Approximate solutions for limiting values of $a_*\equiv a/M$ and b are given in Appendix B. Note that we should exclude the solutions of Eq. (22) which do not satisfy $\dot{t}>0$, where $\dot{t}$ is given by Eq. (12). The results of these calculations are given in Figs. 1 and 2, where we plot r_I as a function of a_* for several b (Fig. 1) and r_I as a function of b for several a_* (Fig. 2) for both prograde and retrograde motions. The left figure in Fig. 2 is the same as [11]. For ISCOs, we find that the sign of $\mathcal{L}$ coincides with the sign of $\dot{\phi}$.

From Fig. 1, we can see that r_I is uniquely determined by a_* and b in the cases of both prograde and retrograde motions. Focusing only on the region $b\geq 0$ (or $b<0$), from Figs. 2 we can see that b, if it exists, is also uniquely determined by a_* and r_I.

III. FATE OF CHARGED PARTICLES KICKED OFF FROM ISCO

We consider the situation where a charged particle is initially in the ISCO but acquires a "kick" by collisions (for example) and then departs from the equatorial plane. The initial velocity is three-dimensional in general, but in order to reduce the space of initial data, we consider as in [14, 19] the kick with transverse velocity $v_\perp\equiv -r_I\dot{\theta}$ without changing $\mathcal{L}$. Even under this restriction, the space of the initial data is large enough to find a wide variety of trajectories. The problem was studied for a non-rotating black hole in [14] and only recently for a rotating black hole in [19], but the analysis was limited to a fixed value of $b(=0.2)$. The slowly rotating case ($a_*=0.5$) was studied by neglecting $O(a_*^2)$ terms in the equation of motion in [15].

More concretely, we numerically solve Eqs. (14) and (15) under the initial conditions

$$r_{\rm ini}\;=\;r_I,\quad \theta_{\rm ini}=\frac{\pi}{2}, \tag{23}$$

$$\dot{r}_{\rm ini}\;=\;0,\quad \dot{\theta}_{\rm ini}=-\frac{v_\perp}{r_I}, \tag{24}$$

where $v_\perp(>0)$ is a constant, and we choose the angular momentum $\mathcal{L}$ as that of ISCO corresponding to the ISCO radius r_I. The energy $\mathcal{E}$ is determined from the normalization condition $u^\mu u_\mu=-1$ as

$$\mathcal{E}\;=\;\frac{4aM\mathcal{L}+\sqrt{r_I^2-2Mr_I+a^2}\sqrt{4\mathcal{L}^2r_I^2+(r_I^3+a^2(2M+r_I))Y}}{2\left(r_I^3+a^2(2M+r_I)\right)}, \tag{25}$$

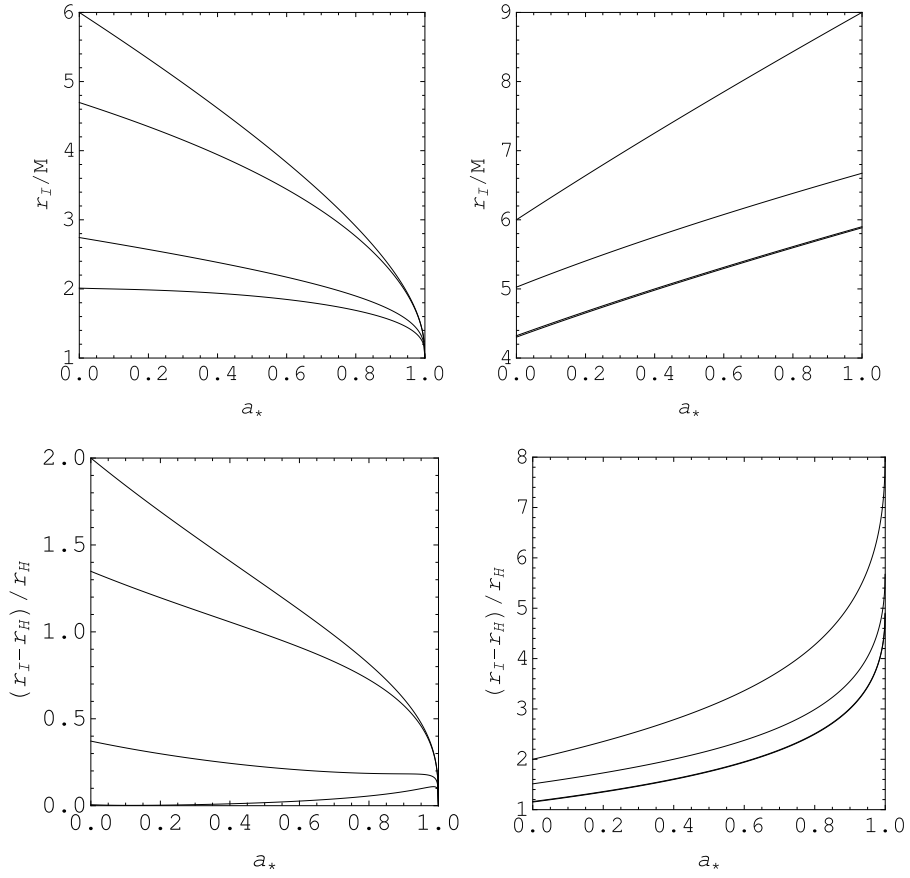

Figure 1: The ISCO radius r_I as a function of a_* for several b. The upper two graphs show the dependence of r_I on a_* for $\mathcal{L} > 0$ (upper left) and for $\mathcal{L} < 0$ (upper right), and the lower two graphs represent the difference between r_I and r_H for $\mathcal{L} > 0$ (lower left) and for $\mathcal{L} < 0$ (lower right). For all graphs, $b = 0, 0.1, 1, 100$ from top to bottom. For $\mathcal{L} < 0$, $b = 100$ curve almost coincides with $b = 10$ curve and is hardly discernible.

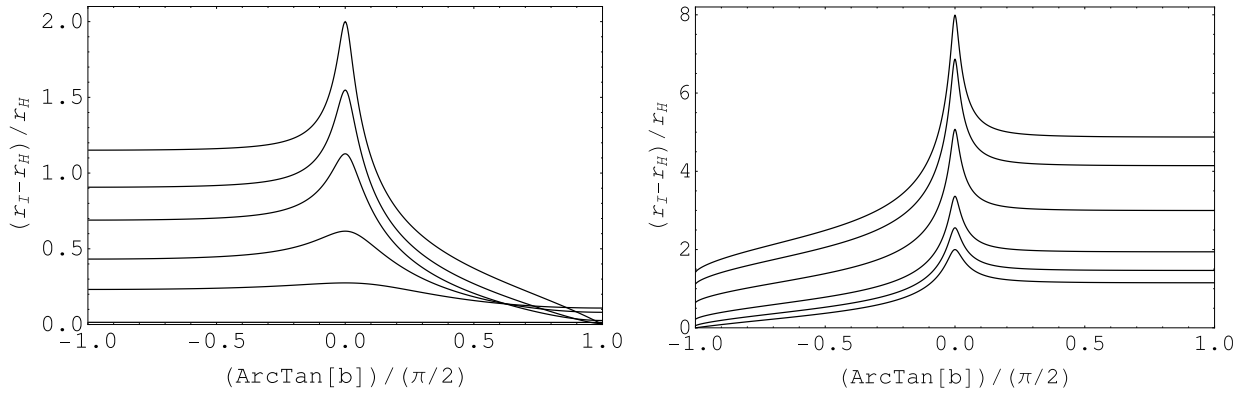

Figure 2: The ISCO radius r_I as a function of $\arctan b$ for several a_* for $\mathcal{L} > 0$ (left) and for $\mathcal{L} < 0$ (right). For $\mathcal{L} > 0$, $a_* = 0, 0.3, 0.6, 0.9, 0.99, 1$ from top to bottom, while from bottom to top for $\mathcal{L} < 0$.

with

$$Y = 4\dot{\theta}_{\rm ini}^2 r_I^3 + (b/M)^2 \left(r_I^3 + a^2(2M + r_I)\right) + 4r_I(1 - b\mathcal{L}/M). \tag{26}$$

For a given a_*, b and $v_\perp$, we solve Eqs. (14) and (15) under the above initial conditions. We assume $b > 0$ in the following. We checked the accuracy of our numerical calculations by verifying constancy of $\mathcal{E}$.

We find that there are four different final states for the particle: capture by the black hole, escape to $z \to \pm\infty$, and bound motion. In our calculations, the maximum integration time was chosen to be $\tau = \tau_{\rm max} = 2M \times 10^5$.

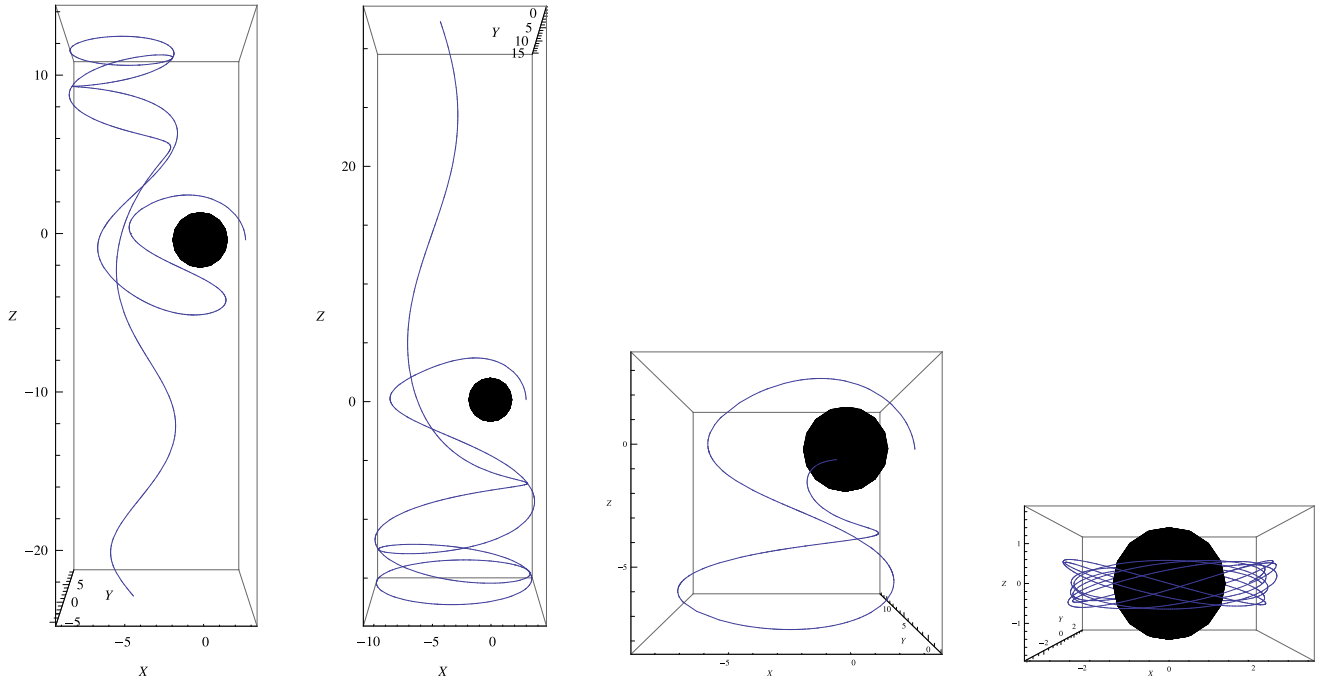

Figure 3: The typical trajectories of the charged particle kicked off from ISCO for prograde motion ($\mathcal{L} > 0$). We set the parameters as $a_* = 0.5, b = 0.24$, and the corresponding ISCO radius is $r_I/M = 3.1081$. The figures are that of $z \to -\infty$ orbit for $\mathcal{E} = 1.24058$ (left), $z \to \infty$ for $\mathcal{E} = 1.90728$ (middle left), capture orbit for $\mathcal{E} = 1.56367$ (middle right) and bound orbit for $\mathcal{E} = 0.761303$ (right), respectively.

We consider the particle to have "escaped" if $|z| > 10^3 M$, "captured" when r reaches r_H, or otherwise in a "bound orbit". Typically, the error in the energy is less than 10^{-6}, but sometimes grows to 10^{-2} when the integration time is very long, which is the case with escape to $|z| \to \infty$ (the increase of the error for the escape orbit was also discussed in [14]). The typical trajectories of the charged particle are depicted in Figs. 3 (for $\mathcal{L} > 0$) and 4 (for $\mathcal{L} < 0$).

Fig. 5 shows the basin of attraction for $\mathcal{L} > 0$ for several a_*. Fig. 6 is for $\mathcal{L} < 0$. The horizontal axis denotes the ISCO radius r_I normalized by M for $b(> 0)$ and the vertical axis denotes the energy $\mathcal{E}$ which is determined from $v_\perp = -r_H \dot{\theta}_{\rm ini}$ using Eqs. (25) and (26). We note that r_I is a function of b for a fixed a_* as shown in Fig. 2. The resolution of the plots in these figures is 300×300. The color of each dot in these figures determines the fate of the particle motion: black for capture, gray for escape to $z \to \infty$, light gray for escape to $z \to -\infty$, and red for bound motion. The white areas correspond to regions forbidden for ISCO orbits. The top left graphs in Figs. 5-6 are for $a_* = 0$ and agree with those in [14].

From Fig. 5, we see that the allowed region becomes smaller as a_* increases. This is because r_I decreases as a_* increases for a fixed b. In particular, $r_I|_{b=0}$ decreases at an almost constant rate but $r_I|_{b=\infty}$ almost coincides with r_H, irrespective of a_* (see Fig. 1). We also find that for the same $\mathcal{E}$ and r_I, the fates of the charged particles are almost the same. The allowed region is gradually "eaten" with increasing a_*. In the $a_* = 0$ figure (top left), the left area (black) corresponds to the region near the black hole horizon, so the orbits are almost all captured. In the right area (gray), r_I is much larger r_H and the effect of the gravity is relatively weak, so the particle can escape to $z \to \infty$ for sufficiently large $v_\perp (> 0)$ as in the case of Minkowski spacetime. The intermediate region looks rather complicated, but it was shown in [14, 19] that the basin of attraction is a fractal. The effect of increasing a_* is to cut the allowed region for $a_* = 0$ from the right.

Similarly, we can understand the features of Fig. 6. This time, the allowed region gets larger as a_* increases. This is because for retrograde ISCOs, r_I increases as a_* increases for a fixed b in contrast to the case of prograde ISCOs. In this case, both $r_I|_{b=0}$ and $r_I|_{b=\infty}$ increase and the difference between them also increases as a_* increases (see Fig 1). Moreover, since r_I of the retrograde motion is larger than that of the prograde motion, the effect of the gravity is rather weak for any a_*. Hence, we expect that the particle can escape to $z \to \infty$ for large $v_\perp$. Thus, the allowed region becomes larger and shifts toward right as a_* increases.

In Figs. 5-6, we plot several red dots between black and white regions. These dots correspond to the bound motion; if the energy is close to that of ISCO, the particle neither escapes to $z \to \pm\infty$ nor is captured by the black hole until at least $\tau = \tau_{\rm max} = 2M \times 10^5$ (these orbits are also observed in [19]). These bound orbits are located around ISCO

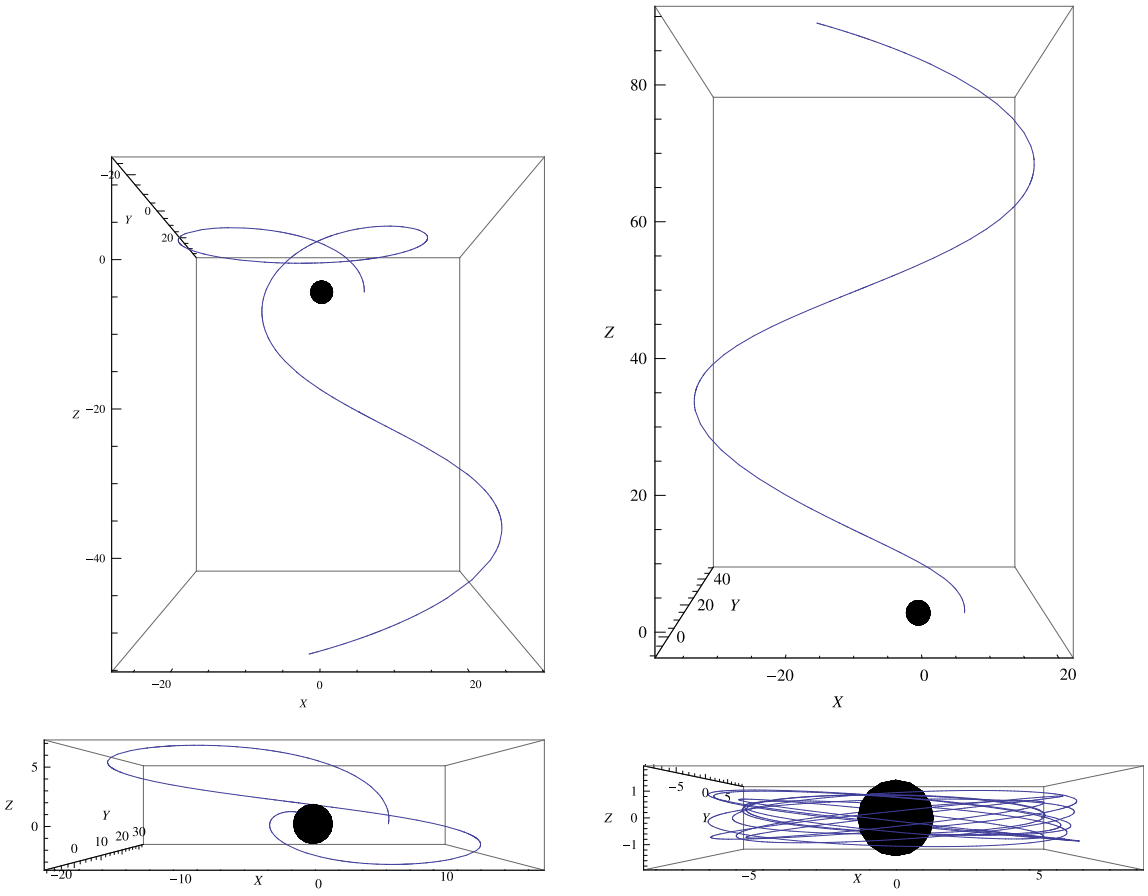

Figure 4: The typical trajectories of the charged particle kicked off from ISCO for retrograde motion ($\mathcal{L} < 0$). We set the parameters as $a_* = 0.5, b = 0.02$, and the corresponding ISCO radius is $r_I/M = 7.2223$. The figures are that of $z \to -\infty$ orbit for $\mathcal{E} = 1.08614$ (upper left), $z \to \infty$ for $\mathcal{E} = 1.17061$ (upper right), capture orbit for $\mathcal{E} = 1.56367$ (lower left) and bound orbit for $\mathcal{E} = 1.00021$ (lower right), respectively.

orbits as shown in the right of Fig. 3. For some of these red dots, we checked that the motion remains bound even if we extend the maximum integration time to $10 \times \tau_{\rm max} = 2M \times 10^6$. The energy error was less than 1.3×10^{-3}. We note that there might exist *quasi*-bound orbits around ISCO which survive for a long time, which may have implications for the high energy particle collision scenario proposed in [11]. We leave the detailed analysis for future work.

IV. SUMMARY

We have studied the motion of charged particles around a weakly magnetized rotating black hole. First, we have studied in detail the effects of black hole spin and an external magnetic field on the ISCOs of charged particles. We found that the radius of the ISCO decreases as the magnetic field increases. Next, we have studied the motion of a charged particle kicked out from the ISCO. We found that trajectories of the particle are full of variety. However, the asymptotic behavior is classified into four types: capture by the black hole, escape to $z \to \pm\infty$, and the bound motion. We found that the final fate depends on the energy of the particle and mainly on the radius of ISCO. The energy and the radius depend on the initial velocity, the black hole spin, and the magnetic field. According to our numerics, particles in bound motion stay in the vicinity of the equatorial plane.

It would be interesting to study the possible existence and stability of bound orbits near the equatorial plane which may widen the region where high energy particle collisions take place [11]. It would also be important to study particle motion in other field configurations and examine the robustness of our results.

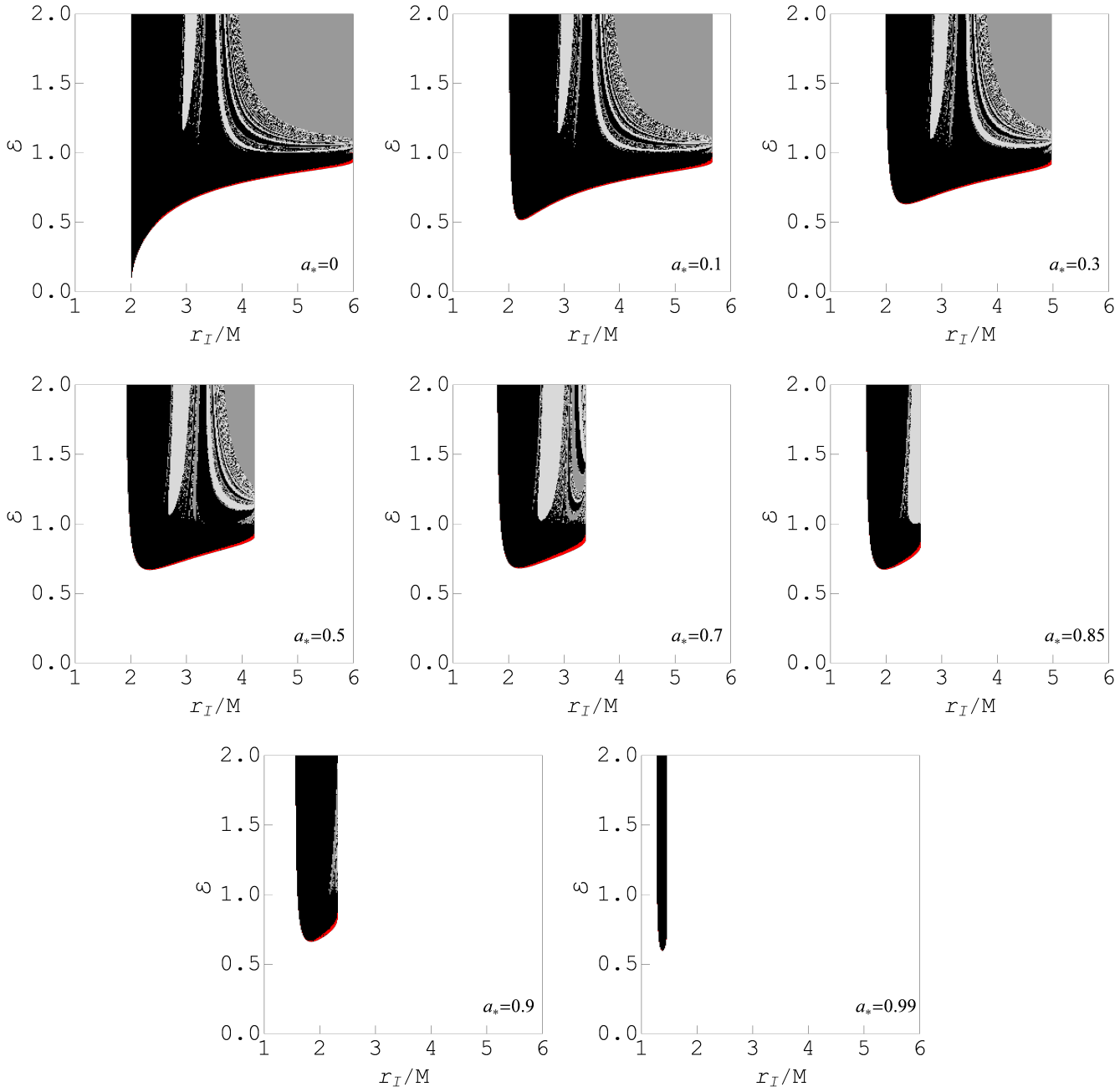

Figure 5: Fate of charged particles kicked off from the prograde ISCO ($\mathcal{L} > 0$) for $a_* = 0, 0.1, 0.3, 0.5, 0.7, 0.85, 0.9, 0.99$ from left to right and down. The dots represent capture (black), escape to $z \to \infty$ (gray), escape to $z \to -\infty$ (light gray) and bound motion (red), respectively. No allowed motion in ISCO in the white area.

ACKNOWLEDGEMENTS

We would like to thank B. Way and the referee for their careful reading of the manuscript and useful comments. We also thank the Yukawa Institute for Theoretical Physics at Kyoto University where this work was initiated during the YITP workshop YITP-X-13-03 on "APC-YITP collaboration: mini-workshop on gravitation and cosmology". This work is supported by the grant for research abroad from JSPS (MK) and by the Grant-in-Aid for Scientific Research from JSPS (Nos. 24540287 (TC)) and in part by Nihon University (RS, TC).

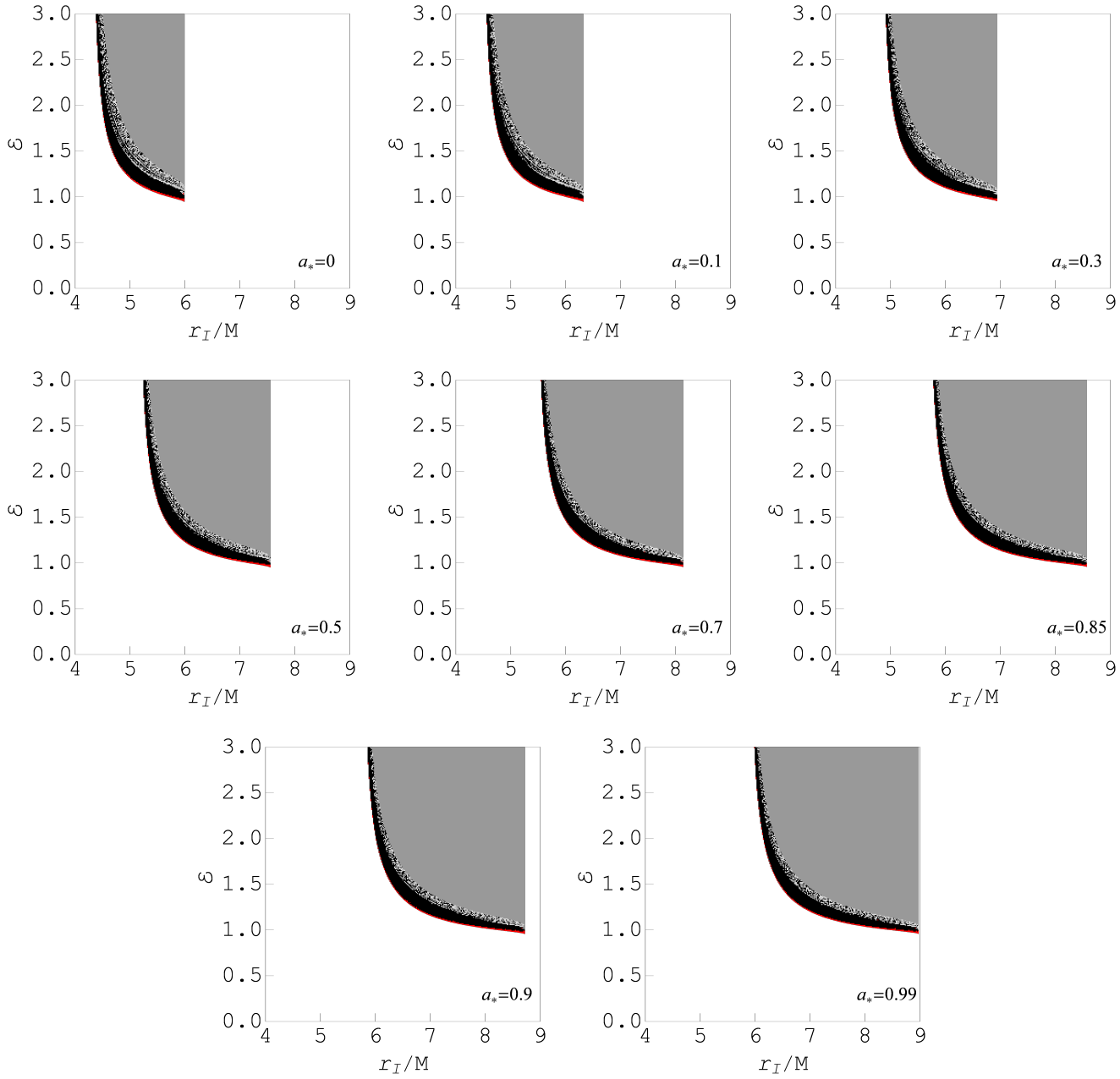

Figure 6: The same as Fig. 5, but for the retrograde ISCO ($\mathcal{L} < 0$).

Appendix A: Magnetic Fluxes Across Black holes

In this appendix, we calculate the flux of an asymptotically uniform magnetic field across one half of the horizon of a rotating black hole. The flux of a magnetic field threading the upper half of the horizon is given by [22]

$$\Phi = \int_0^{2\pi} d\phi \int_0^{\pi/2} d\theta F_{\theta\phi}|_{r=r_H} \,. \tag{A1}$$

For a charge neutral black hole, the 4-vector potential is Eq. (4) and the flux is well-known [22] and is given by

$$\Phi = \pi B r_H^2 \left(1 - \frac{a^4}{r_H^4}\right) = 4\pi B M \sqrt{M^2 - a^2} \,. \tag{A2}$$

The flux decreases as a increases, which is sometimes called a "Meissner-like" effect. However, for a black hole with vanishing electrostatic potential, the 4-vector potential is Eq. (6) and this time the flux is given by

$$\Phi = 4\pi B M^2 \,, \tag{A3}$$

which is *independent* of a. Hence, the presence of a "Meissner-like" effect depends on the choice of the field configuration and does not occur in general.

Appendix B: Approximate solutions for ISCO

Although Eq. (22) can only be solved numerically for general a_* and b, it can be solved analytically for limiting values of a_* and b. However, the previous analyses were limited to the ISCO of a maximally rotating black hole ($a_* = 1$) [10] or to the prograde orbit for a nearly maximally rotating black hole [11]. We extend these analyses to include retrograde motion.

1. ISCO for prograde motion

For a maximally rotating black hole ($a_* = 1$), the radius of the ISCO for a prograde motion ($\mathcal{L} > 0$) is given by [10]

$$r_I^{a_*=1}/M = 1 \,, \tag{B1}$$

independently of b. For a nearly maximally rotating black hole ($a_* \simeq 1$), the correction to Eq. (B1) is [11]

$$r_I/M - r_I^{a_*=1}/M = 2^{2/3}(1-a_*)^{1/3} + \frac{7 + b^2\left(5 - 8b^2 - 6b\sqrt{3+4b^2}\right)}{2^{5/3}\left(1+b^2\right)^2}(1-a_*)^{2/3} + O(1-a_*) \,. \tag{B2}$$

Then $\mathcal{E}$ and $\mathcal{L}$ are given by

$$\mathcal{E} = \frac{\sqrt{3+4b^2}-b}{3} + \frac{2^{2/3}(\sqrt{3+4b^2}-b)^2}{3\sqrt{3+4b^2}}(1-a_*)^{1/3} - \frac{45 - 7b^4 + 4b(3+4b^2)^{3/2}}{2^{5/3}3(3+4b^2)^{3/2}}(1-a_*)^{2/3} + O(1-a_*) \tag{B3}$$

$$\begin{aligned}\mathcal{L}/M = {} & \frac{2(\sqrt{3+4b^2}-b)}{3} + \frac{2^{5/3}(\sqrt{3+4b^2}-b)^2}{3\sqrt{3+4b^2}}(1-a_*)^{1/3} \\ & + \frac{9 + 2b\left(72b + 86b^3 - 5(3+4b^2)^{3/2}\right)}{2^{2/3}3(3+4b^2)^{3/2}}(1-a_*)^{2/3} + O(1-a_*)\end{aligned} \tag{B4}$$

On the other hand, for a Schwarzschild black hole, the ISCO radius for a prograde motion for $b \to \infty$ is given by

$$r_I^{a_*=0}/M = 2 \,. \tag{B5}$$

For a slowly rotating black hole with large b ($1 \gg 1/b \gg a_*$), the correction to Eq. (B5) is [11]

$$r_I/M - r_I^{a_*=0}/M = \frac{2}{\sqrt{3}b} - \frac{8}{9b^2} + \left(-\frac{2}{3^{1/4}b^{1/2}} + O(b^{-3/2})\right)a_* + O(b^{-3}) + O(a_*^2) \,, \tag{B6}$$

and $\mathcal{E}$ and $\mathcal{L}$ becomes

$$\mathcal{E} = \frac{2}{3^{3/4}b^{1/2}} + \left(\frac{b}{2} + O(b^0)\right)a_* + O(b^{-3/2}) + O(a_*^2) \tag{B7}$$

$$\mathcal{L}/M = 2b + 2\sqrt{3} + (-2(3^{3/4})b^{1/2} + O(b^{-1/2}))a_* + O(b^{-1}) + O(a_*^2) \tag{B8}$$

2. ISCO for retrograde motion

We seek a solution to Eq. (22) for a retrograde motion ($\mathcal{L} < 0$). As found by Aliev and Ozdemir [10], in the case a maximally rotating black hole ($a_* = 1$), the radius of the ISCO for a retrograde motion for $b \to \infty$ is given by

$$r_I^{a_*=1}/M = 2 + 4\,\cos\left(\frac{1}{3}\arctan\left(\frac{\sqrt{7}}{3}\right)\right) \simeq 5.884 \,. \tag{B9}$$

For a nearly maximally rotating and a large b (specifically we consider the case $O(1/b^2) \sim O(1-a_*)$), the correction to Eq. (B9) is

$$r_I/M - r_I^{a_*=1}/M = \alpha(1-a_*) + \beta b^{-2} + O(1-a_*)^2 + O(b^{-3}) \tag{B10}$$

$$\begin{aligned}
\alpha &= \frac{8\left(4466012+\sqrt{79916110092053}\cos\left(\frac{1}{3}\arctan\left(\frac{2870281010308837411\sqrt{7}}{5715327328333426410209}\right)\right)\right)}{-25156453+4\sqrt{158178564944911}\cos\left(\frac{2\pi}{3}+\frac{1}{3}\arccos\left(\frac{-324799494986675497691\sqrt{\frac{7}{22596937849273}}}{180775502794184}\right)\right)} \\
&\simeq -1.42114 \\
\beta &= \frac{-22\left(56057+6\sqrt{298562594}\cos\left(\frac{1}{3}\arctan\left(\frac{2220413061871\sqrt{7}}{40850566758917}\right)\right)\right)}{-75469359+12\sqrt{158178564944911}\cos\left(\frac{2\pi}{3}+\frac{1}{3}\arccos\left(\frac{-324799494986675497691\sqrt{\frac{7}{22596937849273}}}{180775502794184}\right)\right)} \\
&\simeq 1.55107\times 10^{-2}\,.
\end{aligned} \tag{B11}$$

The asymptotic form of $\mathcal{E}$ and $\mathcal{L}$ is given by

$$\begin{aligned}
\mathcal{E} &= \left(7.82673b + 8.72195\times 10^{-2}b^{-1}\right) + \left(-2.07312b + 1.80836\times 10^{-2}b^{-1}\right)(1-a_*) \\
&\quad + O(1-a_*)^2 + O(b^{-3}) \qquad \text{(B12)} \\
\mathcal{L}/M &= \left(-42.614b - 0.37131\,b^{-1}\right) + \left(20.0393b + 5.03812\times 10^{-3}b^{-1}\right)(1-a_*) + O(1-a_*)^2 + O(b^{-3})\,, \qquad \text{(B13)}
\end{aligned}$$

which seems to agree with Eq.(43) in [10] although the limiting value of $\mathcal{L}$ slightly deviates from theirs.

On the other hand, for a Schwarzschild black hole, the ISCO radius for a retrograde motion for $b \to \infty$ is given by

$$r_I^{a_*=0}/M = \frac{5+\sqrt{13}}{2} \simeq 4.30278\,. \tag{B14}$$

For a slowly rotating black hole with large b ($1 \gg 1/b \gg a_*$), the correction to Eq. (B14) is

$$r_I/M - r_I^{a_*=0}/M = \sqrt{\frac{107+41\sqrt{13}}{78}}a_* + \frac{1}{234}\left(41\sqrt{13}-143\right)b^{-2} + O(b^{-3}) + O(a_*^2)\,. \tag{B15}$$

Then $\mathcal{E}$ and $\mathcal{L}$ take the forms

$$\begin{aligned}
\mathcal{E} &= \left(\sqrt{\frac{1}{3}\left(46+13\sqrt{13}\right)}b + \frac{1}{6b}\sqrt{\frac{1}{3}\left(\sqrt{13}-2\right)}\right) + \left(\frac{4+\sqrt{13}}{3}b + \frac{\left(-5019+1250\sqrt{13}\right)}{11934b}\right)a_* \\
&\quad + O(b^{-3}) + O\left(a_*^2\right), \qquad \text{(B16)} \\
\mathcal{L}/M &= \left(-\frac{47+13\sqrt{13}}{4}b + \frac{1-\sqrt{13}}{6b}\right) + \left(-\sqrt{\frac{1}{6}\left(1013+281\sqrt{13}\right)}b + \frac{81}{13b}\sqrt{\frac{6}{439183+121829\sqrt{13}}}\right)a_* \\
&\quad + O(b^{-3}) + O(a_*^2), \qquad \text{(B17)}
\end{aligned}$$

which coincide with the results by Frolov and Schoom [13] in the limit of $a_* \to 0$.

[1] M. J. Rees, Ann. Rev. Astron. Astrophys. **22**, 471 (1984).
[2] N. I. Shakura and R. A. Sunyaev, Astron. Astrophys. **24**, 337 (1973).
[3] R. D. Blandford and R. L. Znajek, Mon. Not. Roy. Astron. Soc. **179**, 433 (1977).
[4] A. Tchekhovskoy, R. Narayan and J. C. McKinney, Mon. Not. Roy. Astron. Soc. **418**, L79 (2011).
[5] A. Tchekhovskoy, R. Narayan and J. C. McKinney, Astrophys. J. **711**, 50 (2010) [arXiv:0911.2228 [astro-ph.HE]].
[6] A. C. Fabian, M. J. Rees, L. Stella and N. E. White, Mon. Not. Roy. Astron. Soc. **238**, 729 (1989).
[7] C. S. Reynolds, arXiv:1302.3260 [astro-ph.HE].
[8] S. N. Zhang, W. Cui and W. Chen, Astrophys. J. **482**, L155 (1997)
[9] J. E. McClintock, R. Narayan and J. F. Steiner, arXiv:1303.1583 [astro-ph.HE].
[10] A.N. Aliev and N. Ozdemir, Mon. Not. Roy. Astron. Soc. **336**, 241 (2002).
[11] T. Igata, T. Harada and M. Kimura, Phys. Rev. D **85**, 104028 (2012).

[12] A. R. Prasanna and C. V. Vishveshwara, Pramana **11**, 359 (1978).
[13] V. P. Frolov and A. A. Shoom, Phys. Rev. D **82**, 084034 (2010) [arXiv:1008.2985 [gr-qc]].
[14] A. M. A. Zahrani, V. P. Frolov and A. A. Shoom, Phys. Rev. D **87**, no. 8, 084043 (2013) [arXiv:1301.4633 [gr-qc]].
[15] S. Hussain, I. Hussain and M. Jamil, arXiv:1402.2731 [gr-qc].
[16] G. Preti, Int. J. Mod. Phys. D **18**, 529 (2009).
[17] G. Preti, Phys. Rev. D **81**, 024008 (2010).
[18] V. P. Frolov, Phys. Rev. D **85**, 024020 (2012) [arXiv:1110.6274 [gr-qc]].
[19] A. M. A. Zahrani, arXiv:1407.7069 [gr-qc].
[20] M. Y. Piotrovich, Y. N. Gnedin, S. D. Buliga, T. M. Natsvlishvili, N. A. Silant'ev and A. S. Nikitenko, arXiv:1409.2283 [astro-ph.SR].
[21] R.M. Wald, Phys. Rev. D **10**, 1680 (1974).
[22] A. R. King, J. P. Lasota and W. Kundt, Phys. Rev. D **12**, 3037 (1975); J. Bicak and V. Janis, Mon. Not. Roy. Astron. Soc. **212**, 899 (1985).